An Empirical Study of the Relationship between Seasonal Precipitation and Thermodynamic Environment in Puerto Rico

PAUL W. MILLER

Department of Oceanography and Coastal Sciences, Louisiana State University, Baton Rouge, Louisiana

THOMAS L. MOTE

Department of Geography, The University of Georgia, Athens, Georgia

CRAIG A. RAMSEYER

Department of Geography and Geosciences, Salisbury University, Salisbury, Maryland

ABSTRACT

With limited groundwater reserves and few reservoirs, Caribbean islands such as Puerto Rico are largely dependent on regular rainfall to meet societal and ecological water needs. Thus, the ability to anticipate seasonal rainfall shortages, such as the 2015 drought, is particularly important, yet few reliable tools exist for this purpose. Consequently, interpolated surface precipitation observations from the Daymet archive are summarized on daily, annual, and seasonal time scales and compared to the host thermodynamic environment as characterized by the Gálvez–Davison index (GDI), a convective potential parameter designed specifically for the tropics. Complementing the Daymet precipitation totals, ≥1.1 million WSR-88D volume scans between 2002 and 2016 were analyzed for echo tops ≥ 10 000 ft (~3 km) to establish a radar-inferred precipitation activity database for Puerto Rico. The 15-yr record reveals that the GDI outperforms several midlatitude-centric thermodynamic indices, explaining roughly 25% of daily 3-km echo top (ET) activity during each of Puerto Rico's primary seasons. In contrast, neither mean-layer CAPE, the K index, nor total totals explain more than 11% during any season. When aggregated to the seasonal level, the GDI strongly relates to 3-km ET ($R^2 = 0.65$) and Daymet precipitation totals ($R^2 = 0.82$) during the early rainfall season (ERS; April–July), with correlations weaker outside of this period. The 4-month ERS explains 51% (41%) of the variability to Puerto Rico's annual rainfall during exceptionally wet (dry) years. These findings are valuable for climate downscaling studies predicting Puerto Rico's hydroclimate in future atmospheric states, and they could potentially be adapted for operational seasonal precipitation forecasting.

1. Introduction

Precipitation forecasting in the eastern Caribbean is a critical task because of the societal and ecological implications of below-normal precipitation in this drought-vulnerable region. With little groundwater storage and limited reservoir capacity, deviations from the climatological seasonal precipitation pattern can pose serious human consequences (Rhiney 2015; Van Beusekom et al. 2016). Further, the region is home to 17 tropical montane cloud forests (Aldrich et al. 1997), biologically diverse ecosystems whose endemic species require regular, abundant rainfall for survival (Foster 2001). Both the ecological and societal impacts of below-normal precipitation were poignantly illustrated during the 2015 drought in Puerto Rico (Mote et al. 2017; O'Connell et al. 2018), the most populous island in the chain. With 3.3 million residents and the 2.3-million-person San Juan metro area, the ability to forecast and anticipate seasonal precipitation on the island is vital.

Consequently, the thermodynamic conditions that support precipitation in tropical environments, often in the form of convection, remain a source of contemporary research (e.g., Gálvez and Davison 2016). Though midlatitude convective environments have received abundant attention during the last several decades (e.g., Johns and Doswell 1992; Haklander and Van Delden 2003;

Corresponding author: Paul W. Miller, pmiller1@lsu.edu

Miller and Mote 2018), the transferability of these findings to tropical climates is dubious. Tropical thermodynamic environments are characterized by greater low-level moisture content, trade-wind inversions, weaker vertical wind shear, and a higher melting level and tropopause. Taken together, these differences serve to alter both the dynamical and microphysical processes active in tropical thunderstorm updrafts compared to their midlatitude counterparts, and diminish the transferability of existing, predominantly midlatitude-centric, convective forecasting techniques to the tropics. For instance, abundant low-level moisture results in greater water loading that retards updraft velocity and enhances negative buoyancy. Thus, outflows strengthen and larger wind shears are required to split tropical thunderstorm updrafts compared to midlatitude storms (Wissmeier and Goler 2009). Additionally, James and Markowski (2010) found that the role of midtropospheric moisture on convective intensity varied according to the magnitude of the convective available potential energy (CAPE). For the CAPEs commonly detected in Puerto Rico, for instance, dry air aloft reduced the vigor of convection (James and Markowski 2010), contrary to the prevailing belief of midlatitude forecasters.

Recognizing this need, a new thermodynamic index, the Gálvez–Davison index (GDI), was developed specifically for the tropics (Gálvez and Davison 2016), and has already received attention in weather and climate research (Mote et al. 2017; Donndelinger and Tseng 2018). However, because the initial validation efforts undertaken by Gálvez and Davison (2016) spanned only the 2013 rainy season and compared the GDI to only remotely sensed cold cloud-top area (brightness temperature $< -10°$C), its performance as a seasonal precipitation analysis tool is less clear. Given the need to anticipate drought in the particularly vulnerable eastern Caribbean region, this study will analyze the relationship between the GDI and seasonal precipitation activity, informed by both radar observations and surface precipitation data, over a 15-yr period (2002–16) in Puerto Rico. After presenting the results, a method for leveraging these findings to produce seasonal precipitation forecasts for Puerto Rico is also outlined.

2. Data and methods

Though the goal of this study is to assess the potential of the GDI as a seasonal precipitation analysis tool with the hope it can be eventually leveraged for seasonal forecasts, the index was originally designed to forecast convective activity, not necessarily precipitation.

The depth of precipitation occurring over Puerto Rico is a function of additional factors, such as storm motion, precipitation efficiency, etc., that are not captured by the GDI. Thus, the GDI will first be compared to radar-derived echo tops (ET) as a proxy for convection on a seasonal scale, a metric more fairly assessing its stated purpose. ET data are also advantageous for being spatially continuous over the island and being able to characterize both the coverage and persistence of precipitation features at an earlier stage of the hydrological cycle. Subsequent to the GDI–ET comparison, the index will be correlated against island-wide seasonal precipitation estimates from the Daymet archive (Thornton et al. 2017).

Gridded radar-derived ET estimates were retrieved for the Weather Surveillance Radar-1988 Doppler (WSR-88D) in Puerto Rico (TJUA; Fig. 1a) between 2002 and 2016 from the publicly available National Centers for Environmental Information (NCEI) archive. The ET product is a 4-km resolution estimate of the highest 18.3-dBZ reflectivity height rounded to the nearest 1.5 km MSL increment (5000 ft), up to a maximum altitude of 21.3 km (70 000 ft). This specific radar product was selected because of its skillful filtering of nonprecipitation echoes, a particular advantage in Puerto Rico's mountainous terrain where ground clutter is frequent. The data were processed to yield the total count of ET grid cells ≥ 3.0 km (10 000 ft) in each of the ~1.1 million volume scans during the 15-yr study period (Fig. 1b). The 3.0-km threshold was the lowest ET threshold that showed little visual evidence of ground clutter contamination. In contrast, the radar returns from the higher terrain features of the Cordillera Central and Luquillo Mountains (Fig. 1a) regularly produced erroneous ET estimates of 1.5 km. Additionally, ET estimates higher than 3.0 km suffered from distinct ranging effects, producing areas of poor ET detection driven by the radar's scan strategy (OFCM 2017). Though the ranging effects, manifested as concentric rings of greater 3.0-km ET frequency, are still evident in Fig. 1b, they are subtler than for higher ET thresholds. The 3.0-km ET threshold is low enough to capture nearly all convective precipitation in Puerto Rico, including the 4.5-km ET cells determined by Nesbitt et al. (2006) to contribute nearly half of the island's annual precipitation, though it likely overshoots frontal showers and some trade-wind orographic rainfall (Scholl and Murphy 2014).

Meanwhile, island-wide mean precipitation totals were derived from the Daymet archive (Thornton et al. 2017). Daymet is a 1-km gridded climate product for North America, including Puerto Rico as of version 3 (Fig. 1c). The dataset employs daily precipitation
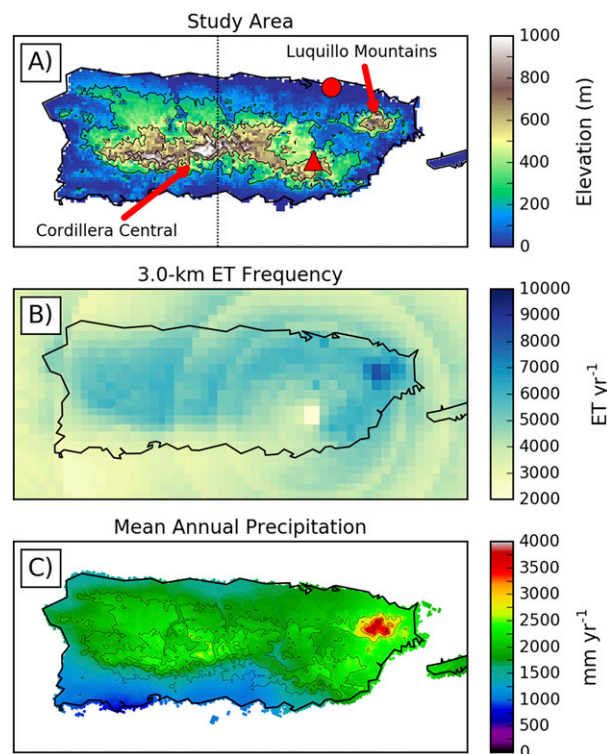
FIG. 1. (a) Topographic map of Puerto Rico with both data collection locations marked. The red circle corresponds to the radiosonde launch site near San Juan, PR (TJSJ), and the red triangle represents the WSR-88D site serving the island (TJUA). The Cordillera Central references the entire east–west oriented mountain chain denoted by the corresponding red arrow. The dashed black line roughly dissecting the island represents the 66.5°W meridian. (b) Annual frequency of ET returns ≥ 3 km for the 15-yr period 2002–16. (c) Annual precipitation climatology for the 30-yr period 1985–2014 from the Daymet dataset.

TABLE 1. Seasonal and annual mean 3-km ET counts and total island-average precipitation as well as the 3-km ET–precipitation R^2 values. The P values determined according to an F test also shown. Annual values are calculated using a December–November year, and as a result, 2002 was dropped from the DS and annual calculations because of missing data.

	DS	ERS	LRS	Annual
3-km ET ($\times 10^6$)	3.8	9.4	13.6	27.8
Precipitation (mm)	344	633	829	1831
ET–precipitation R^2	0.29	0.68	0.69	0.76
ET–precipitation p value	0.05	<0.01	<0.01	<0.01

late rainfall season (LRS; August–November) following the Puerto Rico seasonal delineations of Van Beusekom et al. (2015). Table 1 shows the seasonal contributions to the annual Puerto Rico precipitation and 3-km ET totals as well as the correlation between them. On an annual scale, 3-km ET frequency accounts for 76% of the variation in accumulated precipitation (Table 1), indicating that this radar product is a reasonable measure of Puerto Rico precipitation activity. The seasonal ET frequencies and island-mean precipitation are subsequently compared to the mean GDI value as calculated from the 0000 UTC San Juan, Puerto Rico radiosonde launch (TJSJ; Fig. 1). The 0000 UTC launch time corresponds most closely to the 1900 UTC peak in Puerto Rico diurnal rainfall documented by Jury (2012). Radiosonde observations were retrieved from the publicly accessible Integrated Global Radiosonde Archive (Durre et al. 2006), version 2, maintained by the NCEI.

The GDI calculation, described by Gálvez and Davison (2016), utilizes temperature and specific humidity information at four vertical pressure levels (950, 850, 700, and 500 hPa) to derive three GDI subcomponents: the column buoyancy index (CBI), inversion index (II), and midlevel warming index (MWI). The CBI describes the collocation of heat and moisture in the lower troposphere, which enhances the likelihood of convective activity. Meanwhile, the II captures the prominence of the trade-wind inversion layer, which often serves to extinguish nascent updrafts. Last, the MWI quantifies the destabilizing effect of cool, midlevel troughs versus the stabilizing effect of warm, midlevel ridges on potential convection. The three subcomponents are summed to yield the final GDI, a unitless number typically between −30 and 50 in Puerto Rico. Values between −20 and 5 indicate the potential for shallow convection, with values greater than 5 indicating the potential for brief thunderstorm activity. As the GDI increases above 5, the atmosphere becomes increasingly favorable for deep convection. Readers interested in the full GDI derivation are directed to Gálvez and Davison (2016).

observations from the Global Historical Climatology Network (GHCN) to interpolate a spatially continuous representation of daily precipitation using a truncated Gaussian filter. A validation of the Daymet procedure identified the mean absolute error for precipitation was 19.3% of the annual total (Thornton et al. 1997). Daily Daymet products for Puerto Rico were accessed from 1980 to 2016 to describe daily, seasonal, and annual precipitation totals for the island. Figure 1c shows a clear correspondence between the areas of greatest 3.0-km ET frequency and the regions of greatest annual precipitation accumulation, suggesting that the ET radar product is accurately capturing precipitation-producing features in the atmosphere.

ET frequency and island-mean precipitation totals are summarized during the dry season (DS; December–March), early rainfall season (ERS; April–July), and
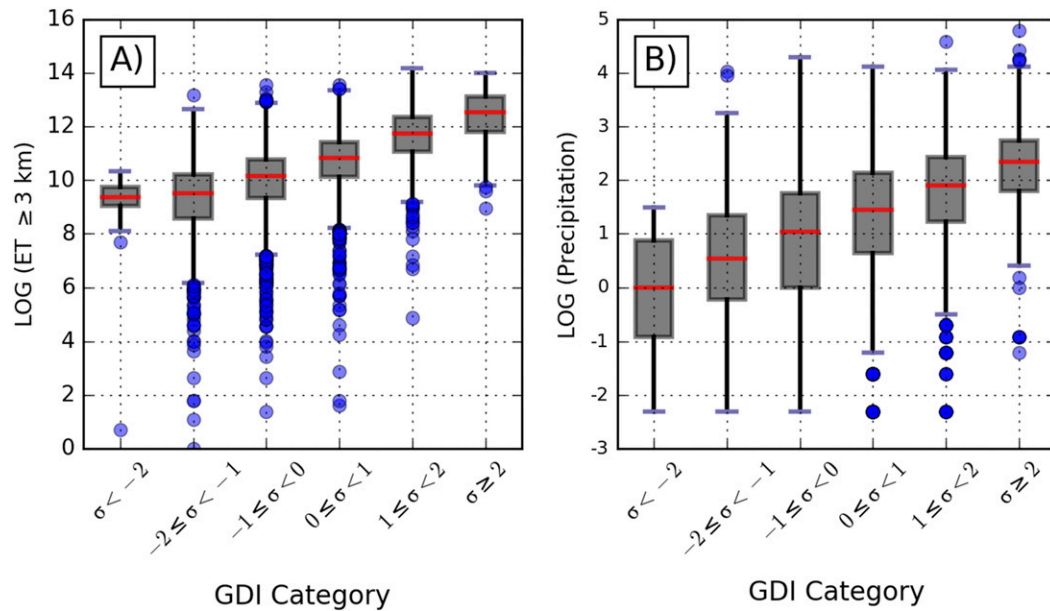
FIG. 2. (a) Daily ET and (b) precipitation activity stratified by GDI value. The six GDI categories are defined by standard deviations ($\sigma = 18.0$) from the mean ($\mu = 1.5$). In ascending order, the average GDI values for each of the categories are -36.7 ($n = 26$), -22.5 ($n = 795$), -7.4 ($n = 2052$), 9.5 ($n = 1446$), 27.3 ($n = 743$), and 42.6 ($n = 185$). Both ET and precipitation are plotted using log axes to facilitate easier visual comparisons.

3. Results

As previously described, the GDI was originally developed as a near-term operational forecasting tool. Thus, before comparing precipitation activity (referring collectively to both 3-km ET frequency and Daymet precipitation totals) against the GDI on a seasonal scale, the GDI will be assessed against both ET and island-wide precipitation on a daily scale. Figure 2 shows that on a daily resolution, higher GDI values (as categorized by standard deviations from normal) are characterized by both more frequent ET $\geq$ 3 km (Fig. 2a) and greater precipitation totals island-wide (Fig. 2b). Additionally, both 3-km ET and daily precipitation increase smoothly with increasing GDI, meaning even small increases in the GDI are associated with greater precipitation activity near Puerto Rico. However, each GDI bin is characterized by a large spread about the median value. Even though GDI increases are associated with increased daily precipitation activity on average, additional factors not explicitly captured by the GDI can lead to enhanced/diminished 3-km ET and/or precipitation activity.

Given Puerto Rico's strongly seasonal climate as described in section 2, the daily GDI performance is disaggregated by season to diagnose any intra-annual trends in performance. Figure 3 shows two sets of linear regression analyses between daily GDI versus 3-km ET

and GDI versus daily precipitation. Though the GDI binning comparison in Fig. 2 depicted considerable intrabin variability for both 3-km ET and precipitation, Fig. 3 shows that the 0000 UTC GDI nonetheless explains ~25% of daily 3-km ET activity during all seasons. In contrast, the correlation between GDI and daily precipitation is weaker. Though the binning analysis in Fig. 2b indicated even clearer increases in rainfall with increasing GDI, this is not reflected in the regression analysis, with GDI explaining only 6%–9% of mean-island precipitation in any season. Because of the large number of days contributing to each R^2 calculation, the relationships are statistically significant even though they are weak and not particularly meaningful.

Figure 4 continues the daily analysis by illustrating the superiority of the GDI as a thermodynamic forecasting tool compared to common, midlatitude-centric parameters. Though Gálvez and Davison (2016) compared the GDI to total totals (TT), the K index (K), and CAPE for a case study, Fig. 4 expands their comparison to a much larger sample, and clearly indicates the value of the GDI over other operational forecasting metrics. For instance, GDI explains 25% of the daily variation in 3-km ET activity during the LRS compared to 1%, 9%, and 3% for mean-layer CAPE (MLCAPE), K, and TT, respectively. The same performance patterns are evident for the ERS; however, during the DS, the performance improvement of the GDI is more modest.
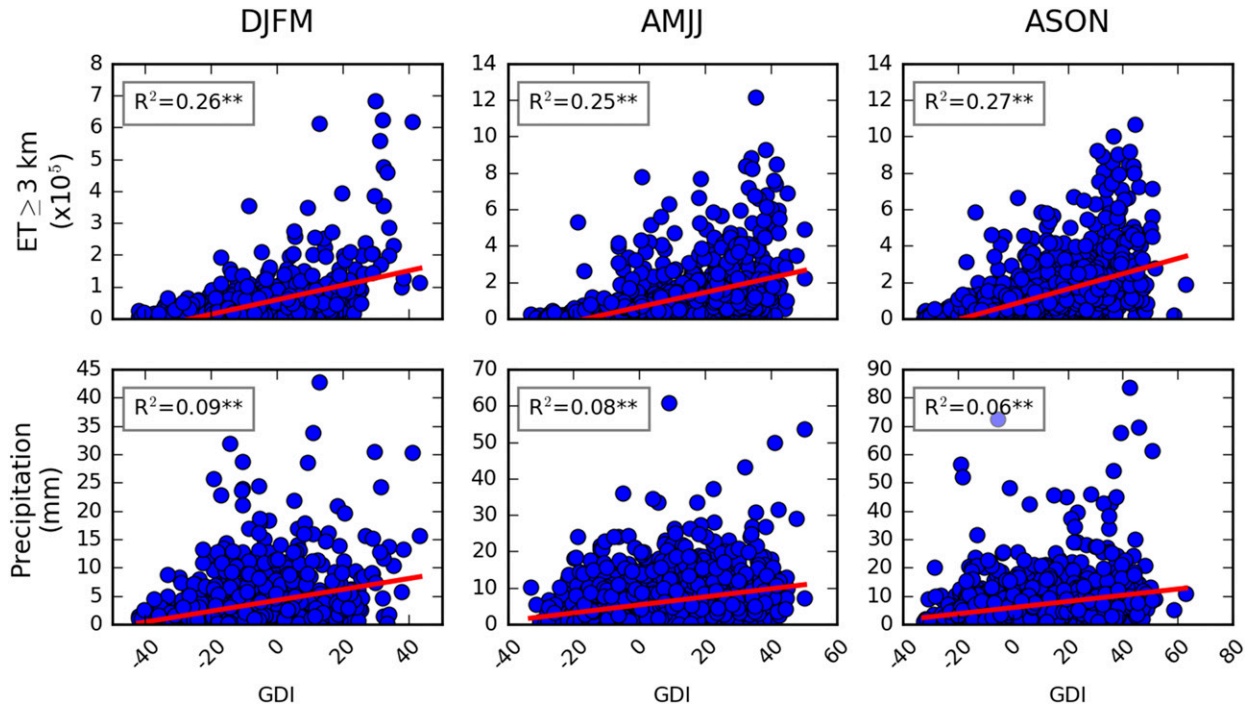
FIG. 3. Scatterplots of (top) daily GDI vs 3-km ET and (bottom) GDI vs precipitation disaggregated according to the three primary seasons in Puerto Rico. Relationships significant at the 95% confidence level according to an *F* test are indicated by an asterisk (*), whereas a double asterisk (**) indicates significance at the 99% confidence level.

During this period of the year, the GDI explains 26% of daily 3-km ET frequency compared to 11% for each mean-layer CAPE, K, and TT. As with Fig. 3, the large number of days contributing to the regression analysis yields statistical significance, even in the absence of strong correlations.

Though the GDI performs as intended on a daily basis, the remainder of the results will be discussed annually and seasonally to assess whether the GDI is a skillful analysis tool on larger temporal scales. Figure 5 relates annual ET $\geq$ 3 km and precipitation totals to the mean annual GDI, and the correlation between the GDI and both precipitation metrics is clear and statistically significant. As with the daily analysis, the GDI is more strongly related to ET returns ($R^2_{ET} = 0.50$; $p < 0.01$) than precipitation. However, on the annual scale, Fig. 5b shows that the GDI nonetheless explains more than one-third ($R^2_{PRCP} = 0.34$; $p < 0.05$) of the variability in mean annual Puerto Rico precipitation compared to 6%–9% when assessed on the daily scale (Fig. 3). Similarly, the GDI explains approximately 25% more of the variation in 3-km ET activity on an annual level than at the daily level.

Though clear relationships are present on the annual and daily levels, the goal of this study is to assess the potential of the GDI as a seasonal precipitation analysis tool. Thus, Fig. 6 first disaggregates the 15-yr 3-km ET dataset by season in attempt to improve upon the performance gains identified by coarsening the temporal (Fig. 5) while still allowing for seasonal skill variation at the coarser interval. The seasonal 3-km ETs are compared against the average GDI for the same period as well as the mean of its three component terms, the CBI, II, and MWI. Within the annual cycle, the GDI is most strongly associated with 3-km ET during the ERS, with correlations substantially weaker and statistically insignificant during the DS and LRS. In fact, the GDI more strongly explains seasonal ERS 3-km ET than both daily ERS 3-km ET and annual ET. However, the opposite pattern is apparent during the LRS. Though the GDI explained 27% of daily 3-km ET variation during the LRS, the relationship is not even statistically significant on the seasonal level.

Breaking down the GDI by component, ET during the ERS are strongly related to the CBI ($R^2_{ERS} = 0.63$), with a coefficient of determination only slightly lower than for the GDI itself ($R^2_{ERS} = 0.65$). Curiously, the MWI displays the opposite relationship to convection from the justification given for its inclusion in the GDI calculation by Gálvez and Davison (2016). As the MWI becomes more negative, 3-km ET frequency increases. However, more negative MWIs correspond to higher
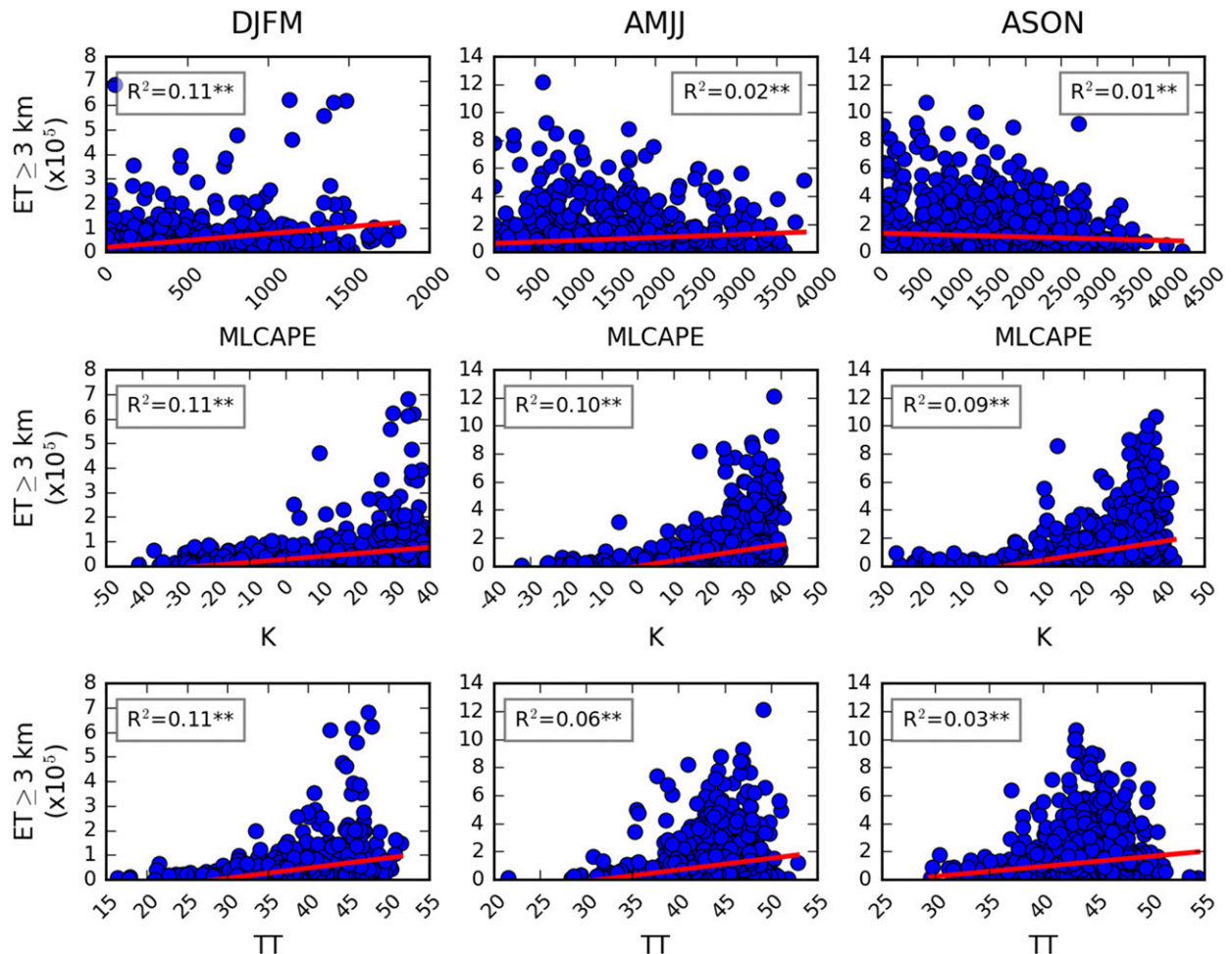
FIG. 4. Scatterplots of three traditional midlatitude thermodynamic parameters [(top) MLCAPE, (middle) K, and (bottom) TT] vs daily 3-km ET. Relationships significant at the 95% confidence level according to an *F* test are indicated by an asterisk (*), whereas a double asterisk (**) indicates significance at the 99% confidence level.

500-hPa temperatures, which are reasoned to limit precipitation by increasing stability as measured by traditional forecasting parameters such as the lifted index. Upon further inspection, the coefficient of determination between the MWI and CBI during the ERS is 0.67 (not shown) with larger CBIs associated with lower (more negative) MWIs. Thus, the propensity for strongly negative MWI environments to host more frequent 3-km ET is likely attributed to the low-level thermodynamic favorability (i.e., high CBI) for tropical convection in these settings.

Working toward the goal of a seasonal precipitation analysis tool, Fig. 7 disaggregates the island-wide-average precipitation by season and compares against the GDI and its subcomponents. As with total 3-km ET, the GDI and precipitation are most strongly correlated during the ERS, with little to no relationship outside of this season. Though correlations during the DS are

weak and statistically insignificant, they are still stronger than the GDI–precipitation relationship during the LRS. Remarkably, there is no relationship between mean GDI and total precipitation during the LRS, the wettest period of the year, despite a statistically significant positive correlation on the daily scale during the same time of year (Fig. 3). In contrast, the coefficient of determination between ERS precipitation and the GDI is an impressive 0.82, greater than that for 3-km ET. This is an unexpected, yet encouraging result given that seasonal precipitation analysis is not an explicitly stated purpose of the GDI.

Though the poor GDI performance on a seasonal scale outside of the ERS is undesirable, the ERS is the most hydrologically critical season, contributing the most variability to annual precipitation anomalies in Puerto Rico. Figure 8 compares the 1980 to 2016 seasonal precipitation anomalies to annual precipitation
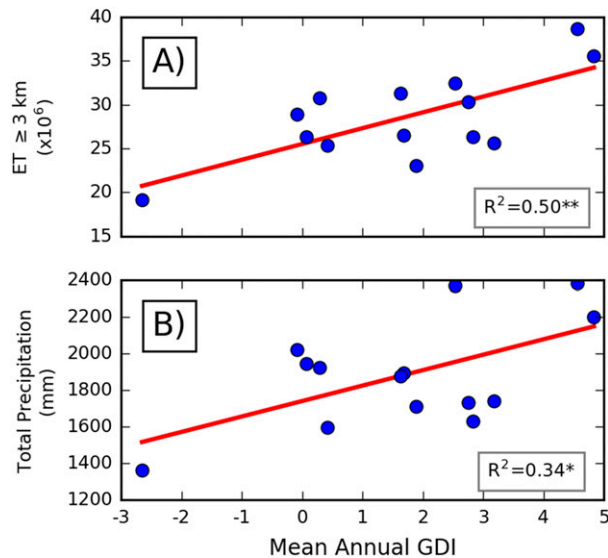
FIG. 5. Annual GDI vs the same measures of precipitation activity in Fig. 2 (averaged annually). A December–November year was employed instead of a calendar year so that each dry season was self-contained to a single annual average, which excluded 2002 (missing December 2001). Relationships significant at the 95% confidence level according to an F test are indicated by an asterisk (*), whereas a double asterisk (**) indicates significance at the 99% confidence level.

anomalies. As expected, variations in the intensity of the two wet seasons (ERS and LRS) explain the most variation in the annual anomaly ($R^2_{LRS} = 0.52$, $R^2_{ERS} = 0.50$, $R^2_{DS} = 0.04$; Fig. 8a). However, when the same relationships are evaluated for only wet years (Fig. 8c) and dry years (Fig. 8d), the ERS anomaly explains much more of the annual outcome than the LRS anomaly. In wet years, the ERS explains 51% of the annual precipitation anomaly ($R^2_{LRS} = 0.15$), and in dry years, it explains 41% of the annual variation ($R^2_{LRS} = 0.13$). Thus, the GDI most accurately characterizes precipitation during the most important period of the year to Puerto Rico's hydroclimate.

4. Discussion

The results presented in section 3 provide ample evidence that the GDI is an improvement to tropical convection forecasting tools than existing midlatitude-oriented thermodynamic indices. During each of the three primary seasons, the GDI explained approximately 25% of the daily variation in 3-km ET frequency, a greater proportion that could be achieved using mean-layer CAPE, TT, or K. The DS, characterized by the most modest GDI performance gains compared to the three traditional tools, is also the time of year when the GDI would not be expected to

perform as capably. Scholl et al. (2009) identified that a larger proportion of DS precipitation in Puerto Rico is attributable to fronts, troughs, and trade-wind orographic precipitation that the GDI is not equipped to capture. Though less frequent in the tropics, these circumstances are common in the midlatitudes where convective parameters like mean-layer CAPE, TT, and K are consulted operationally. Consequently, these indices likely correlated more strongly with daily 3-km ET during the DS (Fig. 4) because this season more resembled the midlatitude environments and associated precipitation mechanisms for which they were developed.

Though the expanded validation in this study corroborated several aspects of the GDI performance in Gálvez and Davison (2016), it also identified some discrepancies. For instance, the CBI term was strongly correlated with both 3-km ET and precipitation, whereas the II and MWI terms were only weakly correlated. In particular, the MWI was negatively correlated with both 3-km ET and total seasonal precipitation. However, the logic applied by Gálvez and Davison (2016) suggests the opposite should be true. The MWI term is a function of 500-hPa temperature with warmer temperatures yielding more negative MWI values. Thus, the pattern documented in Figs. 6–7 during the ERS indicates that precipitation activity increases as the 500-hPa temperature increases, contrary to traditional forecasting logic, which reasons that warmer midlevel temperatures would increase stability (i.e., a more positive lifted index). As section 3 described, the MWI and CBI are strongly negatively correlated during the ERS ($R^2_{ERS} = 0.67$), meaning that as 500-hPa temperatures increase, so does the concentration of heat and moisture in the lower troposphere (i.e., larger CBI). In fact, most shallow convection is likely to be primarily aided by the thermodynamically conducive lower atmosphere, and never penetrate to 500 hPa where the thermodynamic environment is less favorable.

The weak relationship between II and 3-km ET, even during the ERS, was surprising given the relative abundance of literature citing the trade-wind inversion as a limiting factor of tropical convective development (e.g., Cao et al. 2007). Additionally, this layer can be characterized by high dust-aerosol loadings that have been further shown to constrain convective development (e.g., Hosannah et al. 2015; Hosannah et al. 2017). The Saharan air layer (SAL), a plume of hot, dust-rich air advected from Africa to the Caribbean, is associated with larger (i.e., more negative) II values, and was recently shown to play a key role in the historic 2015 Puerto Rico drought (Mote et al. 2017). Similarly, the 2015 ERS witnessed the least number of 3-km ET of all
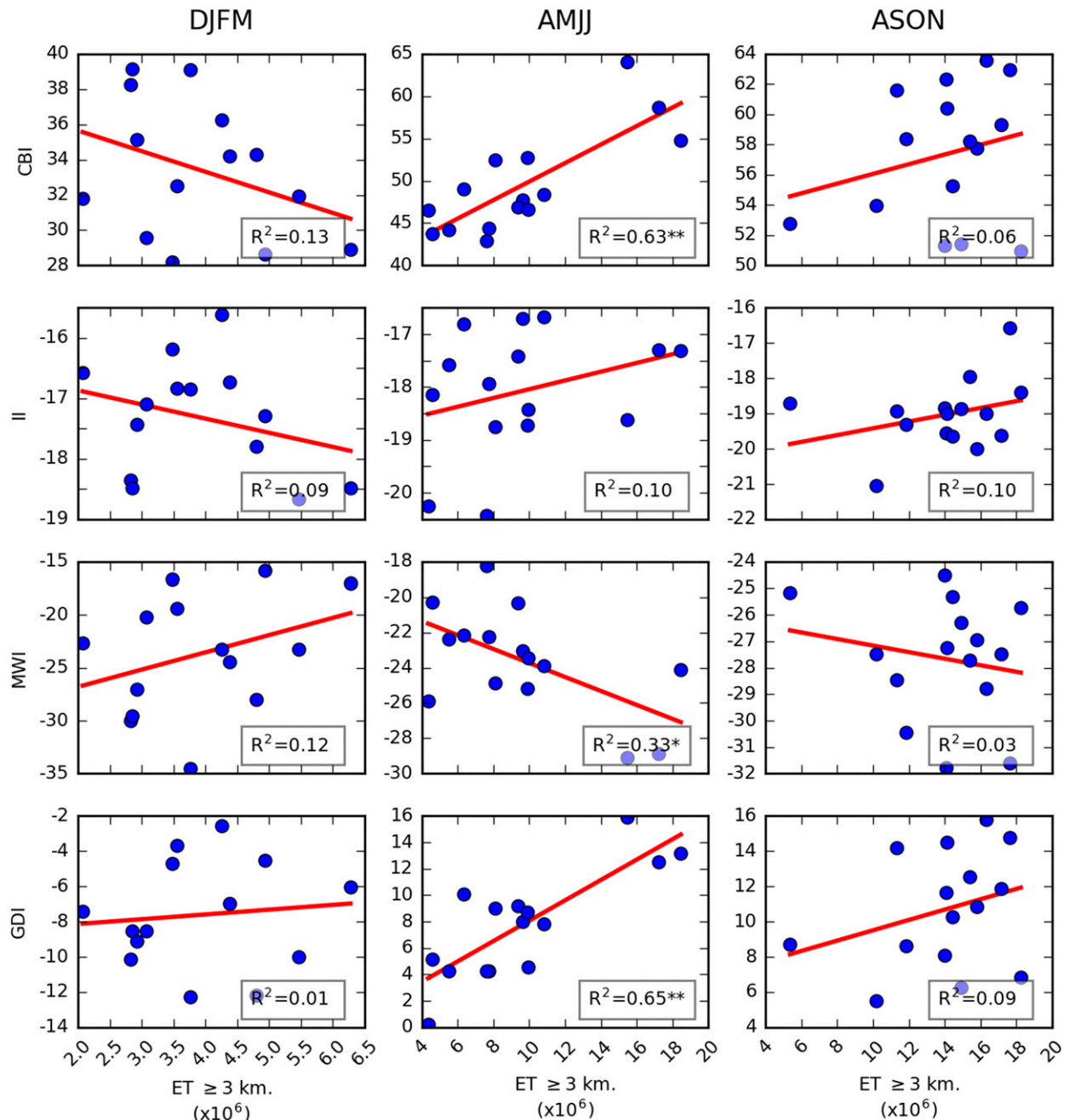
FIG. 6. Seasonal total ET ≥ 3 km vs GDI and its components. Correlations are strongest in the ERS. Relationships significant at the 95% confidence level according to an *F* test are indicated by an asterisk (*), whereas a double asterisk (**) indicates significance at the 99% confidence level.

years in the study period. In addition to preventing nascent updrafts from penetrating this stable layer, established updrafts that encounter the SAL are subject to dry air entrainment, further diminishing their buoyancy. However, neither the II nor the GDI contains a kinematic term describing the negative effects of wind shear on convective development, and thus, may not be fully

describing the detrimental effects of the trade-wind inversion on convection.

Another key finding of this analysis relates to the unexpected decrease in GDI performance when coarsened to the seasonal level during the LRS. Though the GDI performed capably on the daily scale during this time of year, it possessed essentially no skill on the
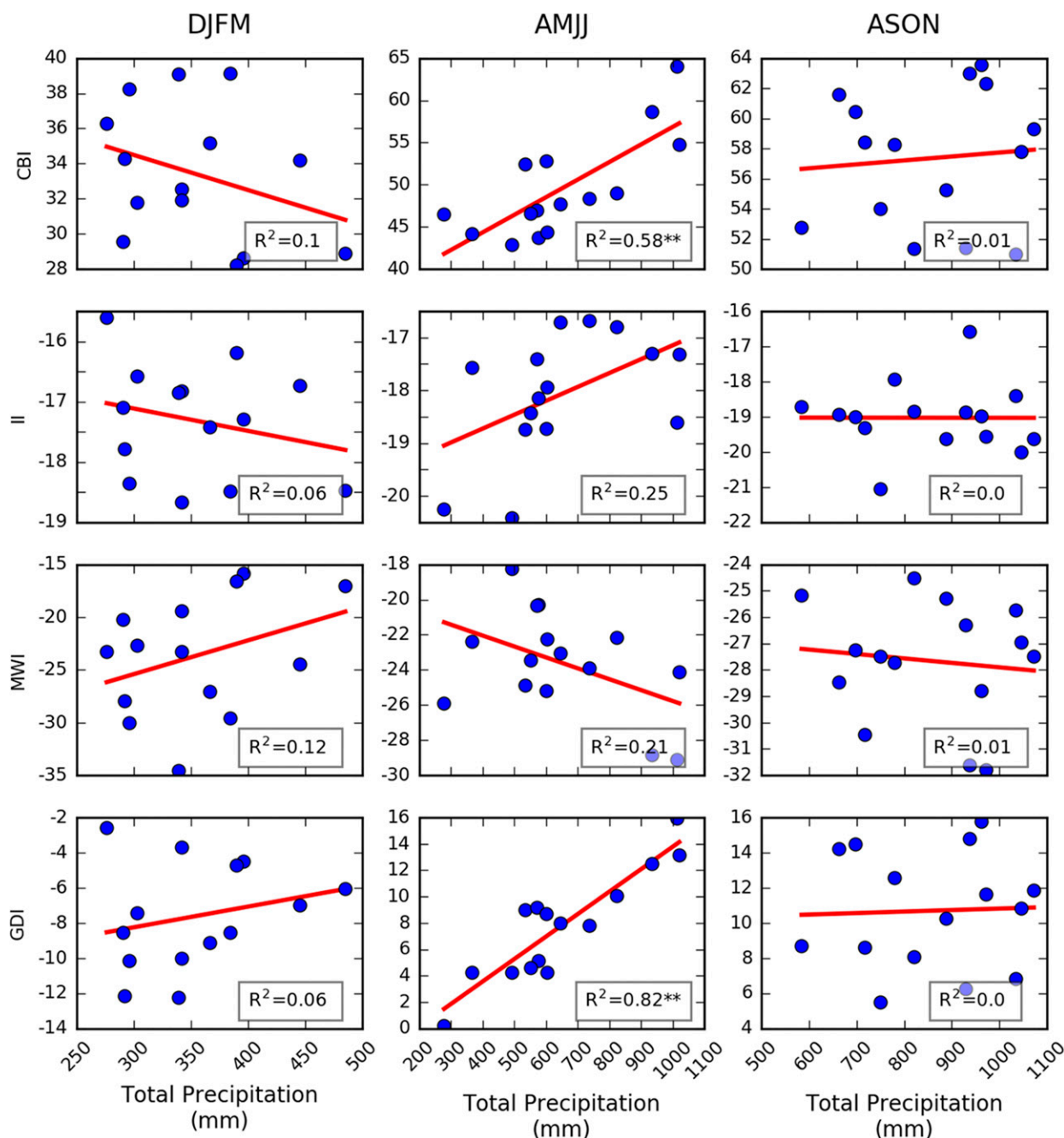
FIG. 7. Seasonal precipitation totals vs GDI and its components. As with convective reflectivities correlations are strongest in the ERS. Relationships significant at the 95% confidence level according to an *F* test are indicated by an asterisk (*), whereas a double asterisk (**) indicates significance at the 99% confidence level.

seasonal level for the same period. Three possible explanations for this result are as follows: 1) the GDI was not developed specifically for Puerto Rico, and the deteriorating relationship outside of the ERS is a function of our location of interest; 2) the synoptic- and meso-scale circulations that favor rainfall in Puerto Rico (Carter and Elsner 1997) vary throughout the annual cycle and can enhance 3-km ET beyond the GDI's expectations at different times of year. For instance, the disproportionate 3-km ET contribution from easterly waves and tropical cyclones on a seasonal level may cause a LRS with a low GDI to possess high 3-km ET count and weaken the regression relationship in Fig. 6; and 3) the 19.3% mean absolute error reported for the
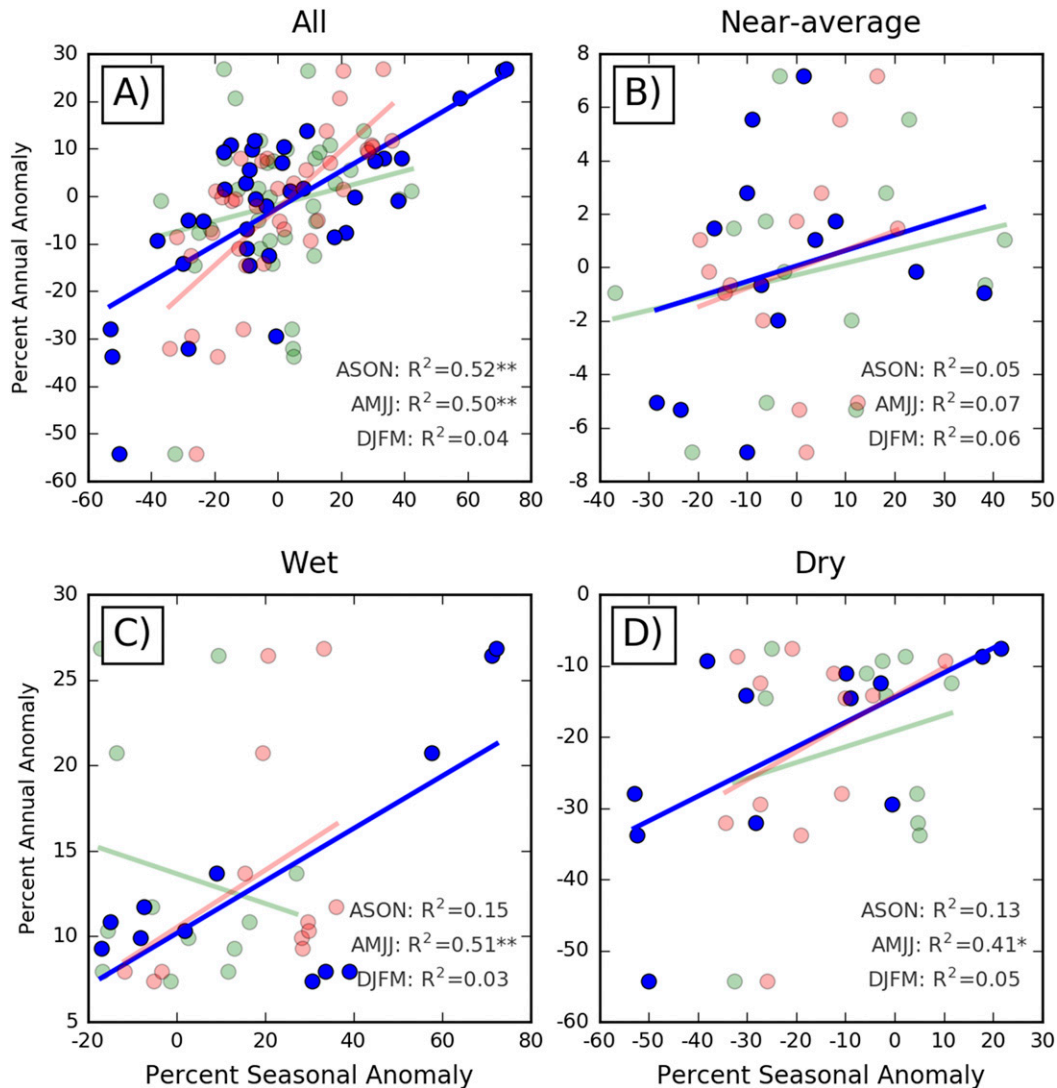
FIG. 8. (a)–(d) Comparison of seasonal precipitation anomalies vs annual precipitation anomalies for all years between 1980 and 2016 based on Daymet island-wide totals. The DS, ERS, and LRS are shown in green, blue, and red, respectively. The least squares linear regression relationships are shown as solid lines of matching color, and the coefficients of determination are located in the bottom right corner of each panel. All 37 years are included in (a), whereas (b)–(d) are stratified by annual totals. Dry (wet) years were identified as the 12 years with the smallest (largest) annual totals, and near-average years represent the 13 years not classified as dry or wet. Relationships significant at the 95% confidence level according to an *F* test are indicated by an asterisk (*), whereas a double asterisk (**) indicates significance at the 99% confidence level.

Daymet dataset (Thornton et al. 1997) would yield higher discrepancies during the LRS compared to the ERS and diminish correlations during this period of the year.

Though not designed for this purpose, the GDI also strongly relates to precipitation during the ERS, explaining 82% of the variation in accumulated ERS rainfall. This performance was aided by several changes in the performance of the GDI subcomponents. For instance, although the II was not statistically significantly related to 3-km ET or precipitation, it was more strongly associated with the latter. One of many possible explanations is that when compared against precipitation, the more negative II may be corresponding to decreases in precipitation efficiency related to dry air entrainment within the inversion layer. According to Gálvez and Davison (2016), the II term is designed to capture dry air entrainment effects within the trade-wind inversion layer, which inhibit warm rain processes in addition to vertical cloud development. Additionally,

the MWI is less closely associated with ERS precipitation, further aiding the GDI's improved performance. Though this sounds counterintuitive, because the MWI is negatively correlated with 3-km ET [instead of positively correlated as Gálvez and Davison (2016) desired], a weaker relationship actually allows the sum GDI to function more like it was originally intended.

By establishing the GDI as a capable ERS precipitation analysis tool and determining the importance of the ERS to Puerto Rico's hydroclimate, this study lays the groundwork for developing the GDI as a seasonal precipitation forecasting aid. Though this study computed the GDI from 0000 UTC TJSJ soundings, the methodology could be adapted to calculate the GDI from proxy soundings extracted from numerical weather model output. For example, the Weather Prediction Center (WPC) already produces 168-h GDI forecasts (https://www.wpc.ncep.noaa.gov/international/gdi/) from the Global Forecast System (GFS). However, this forecast period could be extended to the seasonal scale using simulations from the Climate Forecast System, version 2 (CFSv2; Saha et al. 2014). The 1° resolution CFSv2 is initialized operationally four times daily to produce 9-month global forecasts available at 6-hourly and month-average output resolution. An ensemble of CFSv2 operational runs leading up to the forecast period could be leveraged to produce a probabilistic GDI forecast, which could then be translated into ERS precipitation totals and confidence intervals. Future research should evaluate the ability of the coarse-resolution CFS to predict ERS GDI with an operationally meaningful lead time, and subsequently investigate any necessary bias-correction or calibration procedures.

5. Conclusions

This study analyzes 15 years of 3-km ET and precipitation in Puerto Rico to assess the skill of the Gálvez–Davison index, an operational forecasting measure of convective potential, as a seasonal precipitation analysis tool. The GDI is shown to significantly outperform mean-layer CAPE, the K index, and total totals in corresponding to daily 3-km ET frequencies over the island. This result alone is valuable for weather forecasters in the region attempting to understand daily convective probabilities. Specifically, the GDI explains ~25% of the daily 3-km ET activity during the wettest two-thirds of the year but only 6%–9% of the daily precipitation variability. However, correlations are much stronger on the annual level. The GDI explains 50% of the annual variation in 3-km ET detected by the

Puerto Rico radar station, whereas the relationship with total precipitation is weaker ($R^2_{\mathrm{PRCP}} = 0.34$; $p < 0.05$). Nonetheless, the GDI-precipitation regression relationship in Fig. 5 suggests a decrease (increase) of one GDI unit corresponds to a decrease (increase) of 85 mm in annual total precipitation across the island, equivalent to 765 billion liters of water integrated across the Puerto Rico land area.

When disaggregated by season, the relatively strong daily GDI–ET association during the LRS weakens, and there is essentially no relationship between the GDI and seasonal 3-km ET activity ($R^2_{\mathrm{LRS}} = 0.09$) or precipitation ($R^2_{\mathrm{LRS}} = 0.00$). In contrast, the GDI more accurately characterizes 3-km ET during the ERS ($R^2_{\mathrm{ERS}} = 0.65$) than any other time of year. The relationship becomes even stronger when the GDI is compared against total precipitation during the ERS, explaining 82% of the variation. Fortunately, the ERS is the most influential season in regards to the island's hydroclimate (Fig. 8). ERS rainfall anomalies during wet and dry years are more strongly correlated with annual deviations than any other season. Thus, years with wetter-than-average ERSs tend to be pluvial years, and years with drier-than-average ERSs tend to be drought years. Consequently, the GDI's strong correlation to precipitation and 3-km ET during this season is both desirable and beneficial for future climatological analysis. This finding will aid future climate change studies by isolating the most hydrologically critical period of the year, the ERS, for special attention.

Although the GDI is statistically significantly related to 3-km ET on the daily, seasonal, and annual levels, these relationships leave much room for improvement. For instance, there is essentially no relationship between the GDI and 3-km ET/precipitation during the LRS. Further, the GDI contains no kinematic component, but previous research (Ramseyer and Mote 2018) suggests that the environment's kinematic character also exercises an important control on more shallow and isolated tropical convection. Future research may consider modifying the GDI to include a kinematic component as well as evaluating the ability of coarse-resolution model output, such as the CFSv2, to forecast seasonal GDI values several months in advance. With eastern Caribbean hydroclimates projected to receive less precipitation in the coming decades (Karmalkar et al. 2013; Bhardwaj et al. 2018), the ability to accurately anticipate seasons of below-average precipitation will only become more pressing.

University of Puerto Rico-Rio Piedras to the University of Georgia.

REFERENCES

Aldrich, M., C. Billington, M. Edwards, and R. Laidlaw, 1997: A global directory of tropical montane cloud forests. IUCN-WCMC Rep. 13807, World Conservation Monitoring Centre, Cambridge, United Kingdom, 312 pp.

Bhardwaj, A., V. Misra, A. Mishra, A. Wootten, R. Boyles, J. H. Bowden, and A. J. Terando, 2018: Downscaling future climate change projections over Puerto Rico using a non-hydrostatic atmospheric model. *Climatic Change*, **147**, 133–147, https://doi.org/10.1007/s10584-017-2130-x.

Cao, G., T. W. Giambelluca, D. E. Stevens, and T. A. Schroeder, 2007: Inversion variability in the Hawaiian trade wind regime. *J. Climate*, **20**, 1145–1160, https://doi.org/10.1175/JCLI4033.1.

Carter, M. M., and J. B. Elsner, 1997: A statistical method for forecasting rainfall over Puerto Rico. *Wea. Forecasting*, **12**, 515–525, https://doi.org/10.1175/1520-0434(1997)012<0515:ASMFFR>2.0.CO;2.

Donndelinger, G., and R. Tseng, 2018: A new convective index for Africa. *Eighth Conf. on Transition of Research to Operations*, Austin, TX, Amer. Meteor. Soc., 280, https://ams.confex.com/ams/98Annual/webprogram/Paper328666.html.

Durre, I., R. S. Vose, and D. B. Wuertz, 2006: Overview of the Integrated Global Radiosonde Archive. *J. Climate*, **19**, 53–68, https://doi.org/10.1175/JCLI3594.1.

Foster, P., 2001: The potential negative impacts of global climate change on tropical montane cloud forests. *Earth Sci. Rev.*, **55**, 73–106, https://doi.org/10.1016/S0012-8252(01)00056-3.

Gálvez, J. M., and M. Davison, 2016: The Gálvez–Davison Index for tropical convection. NOAA, 23 pp., http://www.wpc.ncep.noaa.gov/international/gdi/GDI_Manuscript_V20161021.pdf.

Haklander, A. J., and A. Van Delden, 2003: Thunderstorm predictors and their forecast skill for the Netherlands. *Atmos. Res.*, **67–68**, 273–299, https://doi.org/10.1016/S0169-8095(03)00056-5.

Hosannah, N., H. Parsiani, and J. Gonzalez, 2015: The role of aerosols in convective processes during the midsummer drought in the Caribbean. *Adv. Meteor.*, **2015**, 261239, https://doi.org/10.1155/2015/261239.

——, and Coauthors, 2017: The Convection, Aerosol, and Synoptic-Effects in the Tropics (CAST) Experiment: Building an understanding of multiscale impacts on Caribbean weather via field campaigns. *Bull. Amer. Meteor. Soc.*, **98**, 1593–1600, https://doi.org/10.1175/BAMS-D-16-0192.1.

James, R. P., and P. M. Markowski, 2010: A numerical investigation of the effects of dry air aloft on deep convection. *Mon. Wea. Rev.*, **138**, 140–161, https://doi.org/10.1175/2009MWR3018.1.

Johns, R. H., and C. A. Doswell, 1992: Severe local storms forecasting. *Wea. Forecasting*, **7**, 588–612, https://doi.org/10.1175/1520-0434(1992)007<0588:SLSF>2.0.CO;2.

Jury, M. R., 2012: Representation of the Caribbean mean diurnal cycle in observation, reanalysis, and CMIP3 model datasets. *Theor. Appl. Climatol.*, **107**, 313–324, https://doi.org/10.1007/s00704-011-0462-4.

Karmalkar, A. V., M. A. Taylor, J. Campbell, T. Stephenson, M. New, A. Centella, A. Benzanilla, and J. Charlery, 2013: A review of observed and projected changes in climate for the islands in the Caribbean. *Atmósfera*, **26**, 283–309, https://doi.org/10.1016/S0187-6236(13)71076-2.

Miller, P. W., and T. L. Mote, 2018: Characterizing severe weather potential in synoptically weakly forced thunderstorm environments. *Nat. Hazards Earth Syst. Sci.*, **18**, 1261–1277, https://doi.org/10.5194/nhess-18-1261-2018.

Mote, T. L., C. A. Ramseyer, and P. W. Miller, 2017: The Saharan air layer as an early rainfall season suppressant in the Eastern Caribbean: The 2015 Puerto Rico drought. *J. Geophys. Res. Atmos.*, **122**, 10 966–10 982, https://doi.org/10.1002/2017JD026911.

Nesbitt, S. W., R. Cifelli, and S. A. Rutledge, 2006: Storm morphology and rainfall characteristics of TRMM precipitation features. *Mon. Wea. Rev.*, **134**, 2702–2721, https://doi.org/10.1175/MWR3200.1.

O'Connell, C. S., L. Ruan, and W. L. Silver, 2018: Drought drives rapid shifts in tropical rainforest soil biogeochemistry and greenhouse gas emissions. *Nat. Commun.*, **9**, 1348, https://doi.org/10.1038/s41467-018-03352-3.

OFCM, 2017: WSR-88D meteorological observations. Part C: WSR-88D products and algorithms. OFCM Federal Meteorological Handbook FCM-H11C-2017, 394 pp., https://www.ofcm.gov/publications/fmh/FMH11/fmh11partC.pdf.

Ramseyer, C. A., and T. L. Mote, 2018: Analysing regional climate forcing on historical precipitation variability in Northeast Puerto Rico. *Int. J. Climatol.*, **38**, e224–e236, https://doi.org/10.1002/joc.5364.

Rhiney, K., 2015: Geographies of Caribbean vulnerability in a changing climate: Issues and trends. *Geogr. Compass*, **9**, 97–114, https://doi.org/10.1111/gec3.12199.

Saha, S., and Coauthors, 2014: The NCEP Climate Forecast System version 2. *J. Climate*, **27**, 2185–2208, https://doi.org/10.1175/JCLI-D-12-00823.1.

Scholl, M. A., and S. F. Murphy, 2014: Precipitation isotopes link regional climate patterns to water supply in a tropical mountain forest, eastern Puerto Rico. *Water Resour. Res.*, **50**, 4305–4322, https://doi.org/10.1002/2013WR014413.

——, J. B. Shanley, J. P. Zegarra, and T. B. Coplen, 2009: The stable isotope amount effect: New insights from NEXRAD echo tops, Luquillo Mountains, Puerto Rico. *Water Resour. Res.*, **45**, W12407, https://doi.org/10.1029/2008WR007515.

Thornton, P. E., S. W. Running, and M. A. White, 1997: Generating surfaces of daily meteorological variables over large regions of complex terrain. *J. Hydrol.*, **190**, 214–251, https://doi.org/10.1016/S0022-1694(96)03128-9.

——, M. M. Thornton, B. W. Mayer, Y. Wei, R. Devarakonda, R. S. Vose, and R. B. Cook, 2017: Daymet: Daily surface weather data on a 1-km grid for North America, version 3. O. DAAC, accessed 7 March 2018, https://doi.org/10.3334/ORNLDAAC/1328.

Van Beusekom, A. E., G. González, and M. M. Rivera, 2015: Short-term precipitation and temperature trends along an elevation gradient in northeastern Puerto Rico. *Earth Interact.*, **19**, https://doi.org/10.1175/EI-D-14-0023.1.

——, W. A. Gould, A. J. Terando, and J. A. Collazo, 2016: Climate change and water resources in a tropical island system: Propagation of uncertainty from statistically downscaled climate models to hydrologic models. *Int. J. Climatol.*, **36**, 3370–3383, https://doi.org/10.1002/joc.4560.

Wissmeier, U., and R. Goler, 2009: A comparison of tropical and midlatitude thunderstorm evolution in response to wind shear. *J. Atmos. Sci.*, **66**, 2385–2401, https://doi.org/10.1175/2009JAS2963.1.